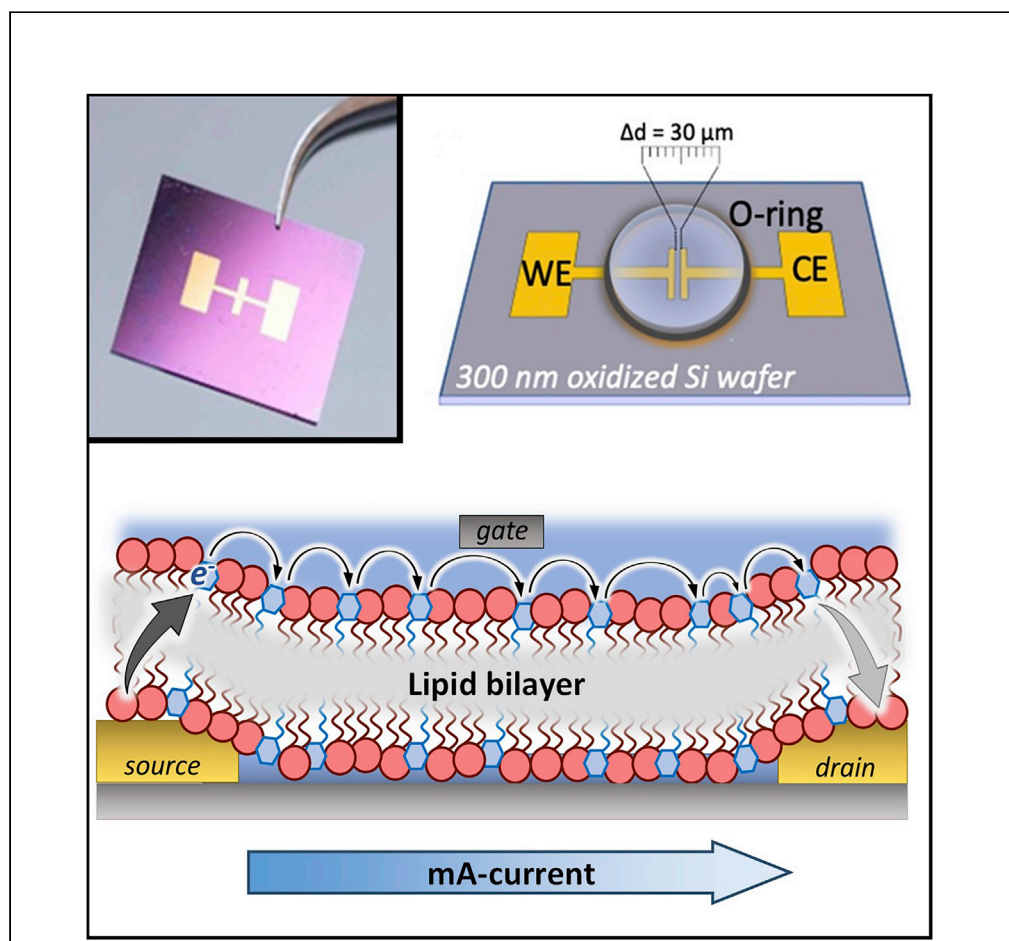**Article**

Q-lipid-containing membranes show high in-plane conductivity using a membrane-on-a-chip setup

Ulrich Ramach,
Jakob Andersson,
Rosmarie
Schöfbeck,
Markus Valtiner

jakob.andersson@ait.ac.at
(J.A.)
valtiner@iap.tuwien.ac.at
(M.V.)

Highlights

Quinone-containing lipid
bilayers show in-plane
conductivity similar to
PEDOT:PSS

In-plane conductivity of
membranes could play a
role in mitochondrial
aging

The process is voltage-
modulated and could be
used for electrolyte-gated
biosensors

Article

Q-lipid-containing membranes show high in-plane conductivity using a membrane-on-a-chip setup

Ulrich Ramach,[1,3,4] Jakob Andersson,[1,2,4,5,*] Rosmarie Schöfbeck,[1] and Markus Valtiner[1,3,*]

SUMMARY

The light-driven reactions of photosynthesis as well as the mitochondrial power supply are located in specialized membranes containing a high fraction of redox-active lipids. In-plane charge transfer along such cell membranes is currently thought to be facilitated by the diffusion of redox lipids and proteins. Using a membrane on-a-chip setup, we show here that redox-active model membranes can sustain surprisingly high currents (mA) in-plane at distances of 25 μm. We also show the same phenomenon in free-standing monolayers at the air-water interface once the film is compressed such that the distance between redox centers is below 1 nm. Our data suggest that charge transfer within cell walls hosting electron transfer chains could be enabled by the coupling of redox-lipids via simultaneous electron and proton in-plane hopping, similar to conductive polymers. This has major implications for our understanding of the role of lipid membranes, suggesting that Q-lipid-containing membranes may be essential for evolving the complex redox machineries of life.

INTRODUCTION

Quinone moieties in molecules of higher life forms are abundant molecular electron, redox, and proton shuttles, serving very diverse purposes.[1] For instance, water-soluble ortho-quinones (Figure 1A) such as adrenaline are important neurotransmitters. The redox chemistry and pH regulation via the amino acid L-*ortho*-Dihydroxyphenylalanin (L-DOPA) plays a central role in wet glues expressed by mussels.[1–4]

Conversely, para-quinones (see Figure 1A) act as amphiphilic "membrane-active" redox-shuttles and coenzymes. For instance, ortho-quinone containing K-vitamins control blood coagulation and support enzymatic activities.[5,6] The thylakoid membrane, which hosts the photosynthetic redox chain, contains plastoquinone (PC) for delivering electrons from photosystem II to plastocyanin, and for building up a proton gradient across the cell membrane.[7,8] In mitochondria, oxidative phosphorylation is supported by co-enzyme Q10.[9,10]

Species-specific Q-coenzymes, shown in Figure 1A, vary in the number of their isoprenoid side chains. For instance, Q10 is the central electron and proton carrier in human mitochondria, whereas *Saccharomyces cerevisiae* use Q6.[11] Hence, membrane-soluble quinones appear as para-quinones in nature, with modestly varying chemistry. Redox membranes are thus electrochemically and conceptually surprisingly similar and conserved across species barriers. They feature a high (up to 30%) content of quinone to provide the reversible redox equilibrium to sustain electron transport chains (ETC).

Based on transmission electron microscopy it has been argued that diffusive electron and proton shuttling via quinones is the major current conduction mechanism along the ETC. The observed swelling of the thylakoid membrane under illumination was linked to enhanced mobility and diffusivity of membrane molecules during photosynthesis.[12] However, diffusion is not rate limiting the ETC from PSII to plastocyanin, but rather the re-oxidation of PC at the plastocyanin redox pocket.[13] Furthermore, electron bifurcation occurs within quinone-membranes (Q-membranes) as a central energy minimization principle for interdependent biologic reaction pathways utilized by nature.[14]

Here, we demonstrate electric, non-diffusive currents across self-assembled co-enzyme Q6-containing membranes ("Q-membranes") in the mA range. A biocompatible material with high in-plane conductivity

[1]Institute for Applied Physics, Vienna University of Technology, 1090 Vienna, Austria

[2]Biosensor Technologies, Austrian Institute of Technology, 1210 Vienna, Austria

[3]Competence Center for Electrochemical, Surface Technologies, CEST, 2700 Wiener Neustadt, Austria

[4]These authors contributed equally

[5]Lead contact

*Correspondence:
jakob.andersson@ait.ac.at
(J.A.),
valtiner@iap.tuwien.ac.at
(M.V.)

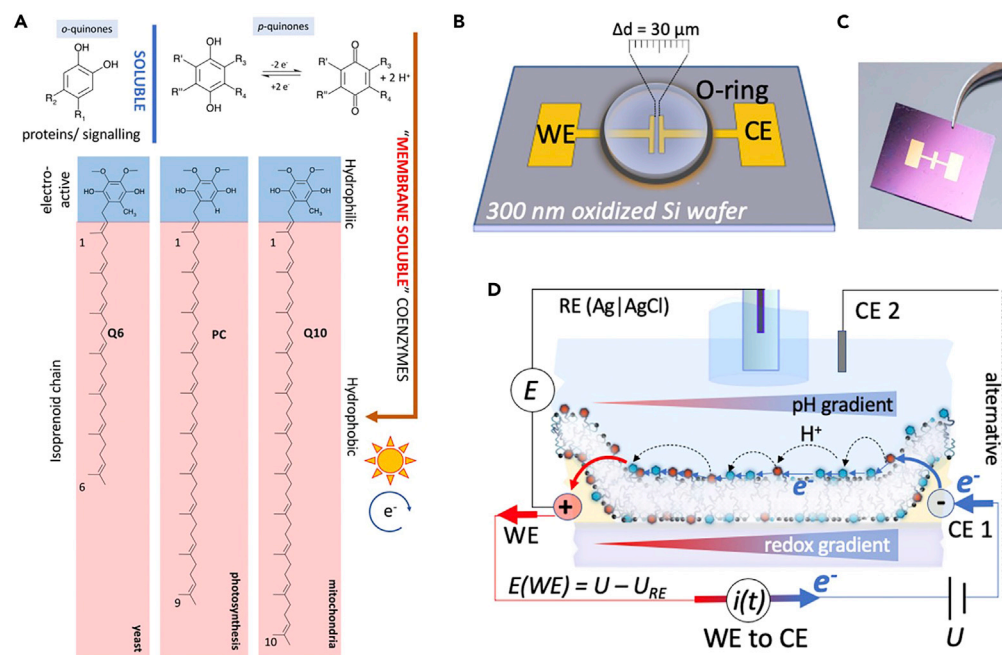https://doi.org/10.1016/j.isci.2022.105918

Figure 1. Structure of redox-active lipids and experimental setup

(A) Water-soluble ortho-quinone motives, general redox reaction of para-quinones as well as the membrane active para-quinones which are linked to hydrophobic isoprenoid chains of varying length (R3).

(B) Schematic of the chip used.

(C) Photograph of the chip.

(D) Schematic of the experimental setup, showing the working (WE), counter (CE1 *or* CE2), and the reference electrode, as well as the deposited lipid bilayer (*c.f.* text for details).

would have an enormous range of applications in bio-electronic materials, for example as interfaces between biological tissues and implants or smart materials and electronic extensions (i.e. smart skin and multisensory input devices). It could also serve as a platform for highly efficient artificial photosynthetic processes and as a biocompatible semi-conducting basis for biosensing devices. For this, we designed an electrochemical *membrane-on-a-chip* setup shown in Figures 1B and 1C. Two electrodes are placed in close proximity (30 μm) on the chip. Using a Langmuir Blodgett trough (LBT), we deposited lipid bilayers at controlled surface pressures. As shown in Figure 1D, the membrane establishes an *in-plane* connection between the two electrodes, allowing us to measure *in-plane* membrane conductivity and resistance.

RESULTS AND DISCUSSIONS

We initially selected a model membrane with 30% (mol) of Q-enzymes (see SI for more information on the materials and methods). As a matrix, the phospholipid 1,2-Distearoyl-*sn*-glycero-3-phosphoethanolamine (DSPE) was used which is not redox active. This matrix lipid has an amine head group facilitating stable membrane coupling to both materials of the sensor. DSPE establishes a lipid bilayer structure with a thickness of about 8 nm,[15] which can naturally host the hydrophobic tail of Q-enzymes, as shown in the schematic in Figure 1A. The formation of stable model membrane architectures with these constituents was tested by LBT and impedance spectroscopy (details see supplemental information, Figures S2–S4, Tables S1 and S2).

As indicated in Figure 2A, we adjusted the redox potential of the working electrode (WE) to a potential of +650 mV vs the RE electrode. Q-coenzymes have a reported primary oxidation peak around 0.2-0.3V,[16,17] which is lower than the potential at which we observed conductivity. However, a large overpotential with an oxidation peak around 0.5 V was also reported for quinones, if they are at some distance from the oxidizing cathode. The distance between the lipid bilayer and the "gating" electrode where the potential was applied is the likely cause of the increased overpotential required to achieve conductivity. As
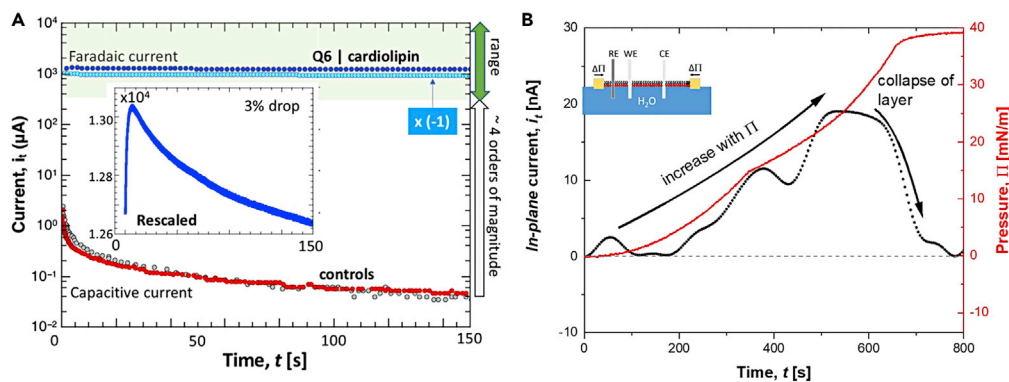
Figure 2. In-plane currents observed on a chip and at the air-water interface

In-plane currents observed on a chip and in monolayers at the air-water interface (A) current between WE and CE1, across 30% Q6|20% cardiolipin|DSPE membranes, in comparison to control measurements with DSPE, and blank chips (data points). Exchanging WE and CE1 reverses the current direction, at a similar magnitude (see x(-1) data). Data for 30% Q6| DSPE is shown in the small re-scaled inset, as well indicated by the observed range (arrow on the right).

(B) Real-time current across a monolayer at the air-water interface comprised of 20% cardiolipin, 30%Q6, and 50% DSPE (black) and correlation with the surface pressure (red). The inset shows a schematic of the measurement setup within the LBT. Additional data on in-plane membrane conductivity and the in-plane current during monolayer compression are shown in Figures S6–S8.

indicated in Figure 2A, this results in a sustained and high oxidation current ranging from 0.3 to 14 mA establishes across the membrane.

These results are only possible if the current is transported along a membrane plane acting like a resistor. If it was diffusion-based, the current would rapidly decline as the charge carrying species are collected at each electrode. We propose that CE1 simultaneously injects electrons, reduces Q-lipids and the *in-plane* current flow maintains the high-level oxidation current at the WE. Hence, an *in-plane* electrochemical current flow across the WE and CE is established, along with a redox gradient. The inset in Figure 2 shows the highest in-plane current we measured in our experiments of 14 mA across membranes containing 30% Q6. Q10 (30%) was also tested, giving similar current ranges.

In Figure 2A, the measured current is compared to control systems not containing Q-enzymes. Measured controls are the blank chip as well as chips deposited with a 100% DSPE membrane. As expected, the pure DSPE membranes and blank chips exhibit a low and expected capacitive charging of the gold WE in the low μA range. In contrast, for Q-membranes, the measured current is ~4 orders of magnitude higher. In principle, this demonstrates a very effective *in-plane* conduction mechanism along the redox-active membrane. However, with this bilayer composition (30% Q-lipid in a matrix of DSPE), we did not obtain a consistent current with one order of magnitude variation of the current from 0.3 to 14 mA across different experiments, sometimes even no conductivity could be achieved. We also found that different lots of Q6/Q10 behaved differently. Specifically, we used chemicals as delivered, and in total 4 different lots (>10 sets of experiments each) were tested. From these patches, three worked and one patch did not yield any significant currents in this configuration (30% Q-enzyme + DSPE).

We postulated that impurities in the naturally extracted material might directly affect the mobility, intra-membrane segregation, and alignment of Q-lipids. Subsequent examination of redox-conducting membranes suggested that the intra-membrane segregation of lipid compounds is further moderated by unsaturated lipids. For instance, in mitochondria, a special lipid known as cardiolipin,[18] with 4 unsaturated 18 carbon long chains, is present with a concentration of up to 20%,[18] while thylakoid membranes contain a similar fraction of branched galactolipids (lipids bearing a sugar head group).[19]

We therefore further explored the effect of cardiolipin close to its natural concentration added to our previous membrane design, i.e. 20% cardiolipin +30% Q6 + 50% DSPE. As Q6-content varies significantly from 3 to 25 μg/g depending on the tissue type,[20] our observations cannot be directly translated into real systems, instead the lipid concentration we chose was used to develop a general understanding of in-plane

charge transfer processes. To understand the function of Q-lipids in specific tissues, model membranes will need to be designed to reproduce the exact lipid compositions found there. When adding cardiolipin, we find consistent currents of up to 1-2 mA for all Q6 batches, including the one that did not work well previously, as shown in Figure 2A. In addition, as shown in Figure S5, AFM imaging of the membranes confirms preferential cluster formation and hence pronounced segregation in membranes without cardiolipin. We, therefore, conclude that the presence of cardiolipin prevents clustering, *i.e.* domain formation. In addition, LBT pressure isotherms indicate a ~35% increased area per molecule in cardiolipin-containing Q-membranes compared to membranes without cardiolipin (Figure S2), similarly indicating less compacted *in-plane* membrane structures. It would be interesting for future studies to examine the impact on *in-plane* current of the area overlap between the lipid bilayer and the electrode as well as the influence on the gap size between the electrodes. We did not examine these factors in the present study, as it would require lengthy changes to the substrate manufacturing process. Moreover, in the presence of cardiolipin, there was a significant difference between the compression and decompression isotherms which we did not observe in films containing only DSPE. To better understand the finding of the observed *in-plane* conductivity, we also examined the electrical behavior of Q-lipid-containing monolayers at the air-water interface in a Langmuir-Blodgett trough (LBT).

The inset in Figure 2B shows a schematic of the designed setup, which allows us to measure conductivity as a function of the 2D lipid surface pressure, i.e. at varying distance and mobility of the lipids at the air-water interface. We expected to measure significantly lower currents in this configuration compared to depositing the bilayer on a chip, as the gap between the electrodes was set to 5 mm rather than 30 μm. However, the large gap size is essential to limit capillary effects between the electrodes at the air-water interface. Experiments were repeated at least in triplicate (see supplemental information for additional data).

Figure 2B shows the effect of the surface pressure on in-plane conductivity of a free-standing monolayer with a similar composition used in the experiments above. The recorded current between two electrodes immersed in the LBT correlates directly with the applied film pressure when a monolayer is freely spanned on the air-water interface between the electrodes. At a pressure of around 5-10 mN/m, where lipid molecules condense from a 2D gas into a liquid phase with distances below 1 nm, we see a significant increase in the in-plane current. Upon further compression, we see a concurrent increase of the current up to 20 nA until a film pressure of 20-35 mN/m is reached. Once the pressure exceeded 35-38 mN/m the current reduced to near zero again. This coincides with the leveling of the surface pressure, at continuous area reduction, which indicates that the monolayer collapses and/or expels Q-lipids from the monolayer as previously proposed.[16,17] This behavior demonstrates that the conductivity of Q-membranes depends on pressure and lipid density, which is in line with previous observations of increased current transduction due to membrane swelling.[12] Furthermore, in monolayers at the air-water interface, the current level decreased by three orders of magnitude compared to the membrane-on-a-chip configuration to the nA-range. This is expected, given that the distance between the electrodes was increased by about three orders of magnitude. This data shows that freestanding Q-lipid monolayers can similarly conduct current and that a membrane-on-a-chip system can utilize these properties.

Hence, membranes, where Q-molecules are better dispersed by the unsaturated lipid fraction, are essential to ensure the consistent mobility and miscibility to establish stable and reproducible "redox-bridging" across such conducting Q-membranes. To further characterize the electrochemical behavior of the bilayer, we analyzed the system with electrochemical impedance spectroscopy (EIS), both across the membrane and along the plane of the membrane. Figure 3A shows a typical *in-plane* potentiostatic impedance spectroscopy of 30% Q6 | 20% cardiolipin|DSPE membranes measured at 650 mV applied to the WE, i.e. during current conduction.

While the in-plane EIS spectrum of a bilayer without Q6 showed a fairly typical EIS spectrum (see Figure 3A) with high resistance, the spectrum of Q6-containing bilayers showed highly unusual behavior similar to redox-active polymer films with negative capacitances attributed to oxidation.[21] Additionally, elements with a negative ohmic resistance were also required to fit the data. The spectrum of the Q6-containing membranes can be fitted with 4 resistor/capacitor (RC) elements in series[22] with an overall resistance of about 400 Ohm (see Figure 3C). For all fitting parameters, see Figure 3D. We chose this model purely for heuristic reasons with the minimum number of parameters needed to graphically fit the data. Currently, the numerical values of the fitted parameters are difficult to interpret due to the large errors. Additional
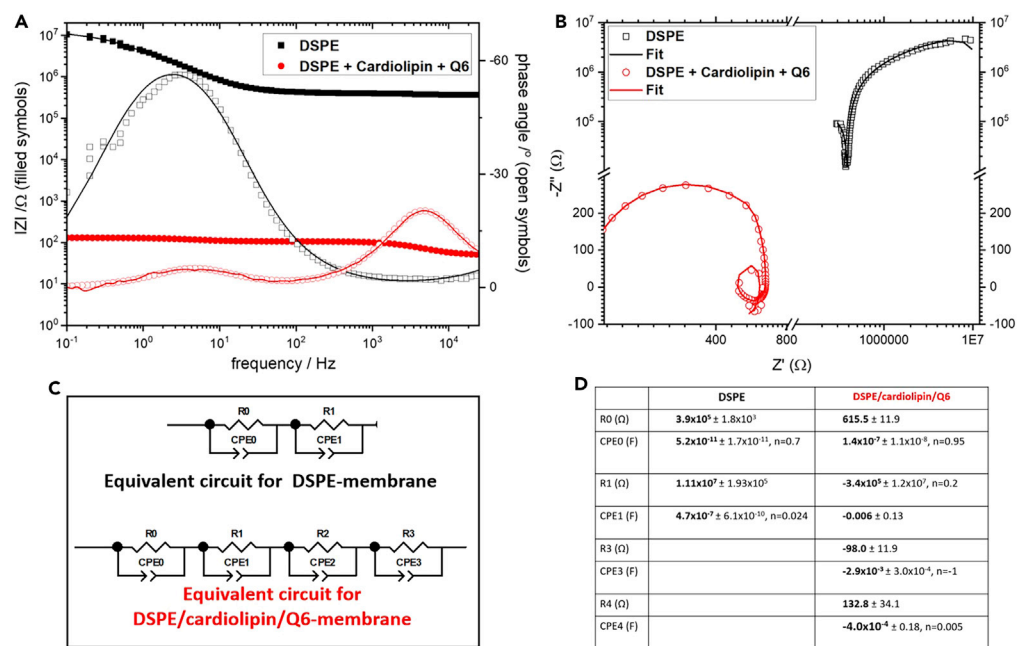
Figure 3. *In-plane* EIS data of a DSPE lipid bilayer and a DSPE/cardiolipin/Q6-membrane

(A) Bode plots of DSPE only (black) and conductive (red) membranes. Symbols represent experimental data and solid lines fitted data.

(B) Complex plots of the same data DSPE only (black) and conductive (red) membranes. Symbols represent experimental data and solid lines fitted data.

(C) Equivalent circuits used to fit the data. D) Fitting parameters for both membrane systems. The errors represent the range of values that could be fitted to each parameter without decreasing the quality of the fit.

studies of the electrochemical properties of this system will be needed to fully understand the phenomena we observed in these measurements. However, the fact that negative resistances and capacitances were observed and necessary to fit this data is indicative of redox phenomena taking place. Considering the time domains, the four RC elements approximate 1) the electron transfer resistance at the gold/membrane interfaces (R3/CPE3), while the other 3 elements at lower frequencies may indicate the coupling of electron flow (described by RE1/2 and CPE1/2) with proton translocation (described by R0/CPE0). This parameter does not occur in Q6-free lipid bilayers as there are no redox processes taking place. The resistance in the high-frequency range in the measurements of the Q6-free bilayer can be attributed to charge transport processes in the water film between the membrane and support.

Interestingly, at lower frequencies, we observe impedance behavior known as an inductive loop[23] (see Figure 3B) which is typically found for ion transport in batteries or fuel cells.[24,25] Such features require seemingly nonphysical negative resistances and/or capacitances for equivalent circuit fits. These are often associated with ionic transport in the direction of the potential, as in this case. We similarly interpret the low-frequency behavior as a consequence of *in-plane* transfer of protons, which enhances the electron transfer (redox) reaction. This eliminates the *in-plane* electron transfer resistance, and the overall circuit resistance appears to originate to a large degree from the transfer resistance of the electrode-membrane coupling (R0) and the proton translocation resistance. Diffusion does not play a significant role, as no diffusion element is necessary to fit the data. The *in-plane* conduction mechanism appears to be complex and will require further investigation before it can be fully understood and technologically utilized.

This interpretation agrees with what we know about biochemical kinetics within ETCs in such membranes. Rate limiting steps are the oxidation/reduction of Q-lipids in protein pockets, rather than electron transfer within the Q-lipid layer.[13] In the absence of Q6, two RC elements are sufficient to describe the data which approximate the bilayer resistance and capacitance and the interface between electrode and electrolyte. In contrast, the vertical resistances of the membranes measured against CE2 (which cannot short circuit with the WE via the membrane) at 650 mV indicate 200-800 of kΩ vertical resistances (also Figures S4 and S3).

This is typical for lipid bilayer membranes, indicating insulating properties in the vertical direction. This is in line with expectations from conducting polymers, where redox centers with distances below 1 nm can contribute to current transduction.[26] For Q-membranes, the distance of redox centers in the vertical direction is around 8 nm given the typical height of a membrane. This limits vertical current flow, by the structural motive. Furthermore, the overall *in-plane* resistance of membranes consisting of DSPE only (control) is in the range of 50 MΩ (Figure S5). This resistance can largely be attributed to the conductivity of the hydration layer underneath the membrane.

Using a typical bilayer height of 5 nm[15] and the electrode width $L = 5$ mm, as well as the electrode distance of 30 μm, the overall resistance R ∼ 400 Ω translates into a specific resistance of $\rho = R_0 A/L = 5 \cdot 10^{-2} [\Omega \cdot m]$. This is lower compared to *e.g.* non-doped silicon and comparable to germanium, GaAs. Conductive polymers are less conductive than the q-lipid-containing bilayers presented here,[27] while enhanced PEDOT:PSS polymers are in the same range of conductivity while being roughly an order of magnitude thicker.[28] The observed conduction mechanism appears similar to charge diffusion in redox polymers, which involves an electron-hopping process from site to site where transport of both electrons and charge-compensating counter-ions occurs simultaneously. The distance between adjacent redox sites is the key factor governing the efficiency of the electron transfer processes in the film. The average area per molecule can be obtained from the Pressure/area curves seen in Figure S2 and is 0.8 nm^2 for our deposition conditions. This corresponds to an average hopping distance between molecules of less than 1 nm and is in accordance with literature expectations for multistep hopping distances across redox-centres.[26]

Based on the impedance data, Figure S9 shows a schematic molecular interpretation of the current conduction. Essentially, electrons and protons simultaneously move in the plane along quinone, semi-quinone, and hydroxy-quinone in self-assembling Q-lipid redox chains. Conceptually, this is likely similar to bacterial nano-wires,[29,30] where the $Fe^{2+}|Fe^{3+}$ redox-couple may transmit current. This may manifest itself in a pH gradient along the plane of the membrane, which should be investigated in future studies.

Summary

In summary, fluid redox-active membranes are good and reliable self-assembling conductors based on proton/electron hoping mechanisms. They can be made highly robust by including polymerizable lipids or amphiphilic block copolymers. These materials could play an important role in future bioelectronic and sensing applications and as an interface between biological and electronic elements (i.e. implants, "smart skin" and human-machine interface technologies.). Purely lipid-based systems likely would be too fragile for this purpose, but by combining lipids with amphiphilic block copolymer systems and possibly some degree of cross-linking, sufficient stability might be reached.

Deterioration of membrane conductivity pathways via loss of quinone activity could be a contributing factor in aging processes.[31] Furthermore, redox-active membranes/liposomes are a potential initial step toward constructing complex ETCs, given that quinone-membranes are conceptually surprisingly similar across species barriers and symbiotically acquired in higher developed life forms,[32] with well-conserved lipid compositions.[33] With more complex n-electrodes setups interdependent ETCs can be studied. One could exploit such membrane architectures and transient redox wiring for making self-assembling "living" electronics.

This study has several limitations. For example, as stated earlier, it is impossible to design the model system such that it represents every type of q-lipid-containing membranes because the content varies considerably. In-plane conductivity may only arise in membranes with particularly large amounts of q-lipids or those containing particular lipid mixtures. There may also be a large temperature dependence on any conductivity phenomena, depending on the lipid mixtures. Finally, this is only a phenomenological description of the charge transport processes. The equivalent circuit we chose to fit the data qualitatively indicates that there are redox phenomena taking place in these membranes, but the circuit may not be completely accurate and as it currently is, no quantitative conclusions about the oxidation rate or mechanism can be drawn. Investigating these phenomena more closely will be essential to better understand these phenomena.

STAR★METHODS

Detailed methods are provided in the online version of this paper and include the following:

- KEY RESOURCES TABLE

- RESOURCE AVAILABILITY
  - Lead contact
  - Materials availability
  - Data and code availability
- METHOD DETAILS
  - Key resources
  - Langmuir - Blodgett transfer
  - Chip production
  - Electrochemistry
  - In-plane conductivity of lipid monolayer at the air-water interface of a Langmuir-Blodgett-Trough
  - Atomic force microscopy
- QUANTIFICATION AND STATISTICAL ANALYSIS

SUPPLEMENTAL INFORMATION

Supplemental information can be found online at https://doi.org/10.1016/j.isci.2022.105918.

AUTHOR CONTRIBUTIONS

U.R. and R.S. performed experiments. J.A. conducted experiments, analyzed impedance data, and supported the conceptual development. M.V. conceptually developed this work.

DECLARATION OF INTERESTS

The Authors declare no competing Interests.

INCLUSION AND DIVERSITY

We support inclusive, diverse, and equitable conduct of research.

REFERENCES

1. Waite, J.H. (2016). The DOPA ephemera: a recurrent motif in invertebrates. Biol. Bull. https://doi.org/10.2307/1542421.

2. Guo, Q., Chen, J., Wang, J., Zeng, H., and Yu, J. (2020). Recent progress in synthesis and application of mussel-inspired adhesives. Nanoscale *12*, 1307–1324. https://doi.org/10.1039/C9NR09780E.

3. Waite, J.H. (2002). Adhesion ıfmmode\gravea\elseà\fi la Moule. Integr. Comp. Biol. *42*, 1172–1180. https://doi.org/10.1093/icb/42.6.1172.

4. Lee, B.P., Messersmith, P.B., Israelachvili, J.N., and Waite, J.H. (2011). Mussel-Inspired adhesives and coatings. Annu. Rev. Mater. Res. *41*, 99–132. https://doi.org/10.1146/annurev-matsci-062910-100429.

5. DiNicolantonio, J.J., Bhutani, J., and O'Keefe, J.H. (2015). The health benefits of vitamin K. Open Heart *2*, e000300. https://doi.org/10.1136/openhrt-2015-000300.

6. Shearer, M.J., and Newman, P. (2008). Metabolism and cell biology of vitamin K. Thromb. Haemost. *100*, 530–547.

7. Junge, W. (2019). Oxygenic photosynthesis: history, status and perspective. Q. Rev. Biophys. *52*, e1. https://doi.org/10.1017/S0033583518000112.

8. Zhao, L.-S., Huokko, T., Wilson, S., Simpson, D.M., Wang, Q., Ruban, A.V., Mullineaux, C.W., Zhang, Y.-Z., and Liu, L.-N. (2020). Structural variability, coordination and adaptation of a native photosynthetic machinery. Nat. Plants *6*, 869–882. https://doi.org/10.1038/s41477-020-0694-3.

9. Osellame, L.D., Blacker, T.S., and Duchen, M.R. (2012). Cellular and molecular mechanisms of mitochondrial function. Best Practice & Research. Best Pract. Res. Clin. Endocrinol. Metab. *26*, 711–723. https://doi.org/10.1016/j.beem.2012.05.003.

10. Friedman, J.R., and Nunnari, J. (2014). Mitochondrial form and function. Nature *505*, 335–343. https://doi.org/10.1038/nature12985.

11. Parapouli, M., Vasileiadis, A., Afendra, A.-S., and Hatziloukas, E. (2020). Saccharomyces cerevisiae and its industrial applications. AIMS Microbiol. *6*, 1–31. https://doi.org/10.3934/microbiol.2020001.

12. Kirchhoff, H., Hall, C., Wood, M., Herbstová, M., Tsabari, O., Nevo, R., Charuvi, D., Shimoni, E., and Reich, Z. (2011). Dynamic control of protein diffusion within the granal thylakoid lumen. Proc. Natl. Acad. Sci. USA. *108*, 20248–20253. https://doi.org/10.1073/pnas.1104141109.

13. Crofts, A.R., Hong, S., Wilson, C., Burton, R., Victoria, D., Harrison, C., and Schulten, K. (2013). The mechanism of ubihydroquinone oxidation at the Qo-site of the cytochrome bc1 complex. Biochim. Biophys. Acta *1827*, 1362–1377. https://doi.org/10.1016/j.bbabio.2013.01.009.

14. Yuly, J.L., Zhang, P., Lubner, C.E., Peters, J.W., and Beratan, D.N. (2020). Universal free-energy landscape produces efficient and reversible electron bifurcation. Proc. Natl. Acad. Sci. USA. *117*, 21045–21051. https://doi.org/10.1073/pnas.2010815117.

15. Israelachvili, J.N. (2011). Intermolecular and Surface Forces (Academic Press).

16. Hoyo, J., Guaus, E., Torrent-Burgués, J., and Sanz, F. (2012). Electrochemical behaviour of mixed LB films of ubiquinone–DPPC. Journal of electroanalytical chemistry *669*, 6–13.

17. Hoyo, J., Guaus, E., Torrent-Burgués, J., and Sanz, F. (2015). Electrochemistry of LB films of mixed MGDG: UQ on ITO. Bioelectrochemistry *104*, 26–34.

18. Schlame, M., Rua, D., and Greenberg, M.L. (2000). The biosynthesis and functional role of cardiolipin. Prog. Lipid Res. *39*, 257–288. https://doi.org/10.1016/S0163-7827(00)00005-9.

19. Dörmann, P., and Benning, C. (2002). Galactolipids rule in seed plants. Trends Plant Sci. *7*, 112–118. https://doi.org/10.1016/S1360-1385(01)02216-6.

20. Turunen, M., Olsson, J., and Dallner, G. (2004). Metabolism and function of coenzyme Q. Biochim. Biophys. Acta *1660*, 171–199.

21. Chen, W.-C., Wen, T.-C., and Gopalan, A. (2002). Negative capacitance for polyaniline: an analysis via electrochemical impedance spectroscopy. Synth. Met. *128*, 179–189.

22. Schönleber, M., and Ivers-Tiffée, E. (2015). Approximability of impedance spectra by RC elements and implications for impedance analysis. Electrochem. Commun. *58*, 15–19. https://doi.org/10.1016/j.elecom.2015.05.018.

23. Klotz, D. (2019). Negative capacitance or inductive loop? – a general assessment of a common low frequency impedance feature. Electrochem. Commun. *98*, 58–62. https://doi.org/10.1016/j.elecom.2018.11.017.

24. Setzler, B.P., and Fuller, T.F. (2015). A physics-based impedance model of proton exchange membrane fuel cells exhibiting low-frequency inductive loops. J. Electrochem. Soc. *162*, F519–F530. https://doi.org/10.1149/2.0361506jes.

25. Roy, S.K., Orazem, M.E., and Tribollet, B. (2007). Interpretation of low-frequency inductive loops in PEM fuel cells. J. Electrochem. Soc. *154*, B1378. https://doi.org/10.1149/1.2789377.

26. Pirbadian, S., and El-Naggar, M.Y. (2012). Multistep hopping and extracellular charge transfer in microbial redox chains. Phys. Chem. Chem. Phys. *14*, 13802–13808. https://doi.org/10.1039/C2CP41185G.

27. Karpov, Y., Erdmann, T., Raguzin, I., Al-Hussein, M., Binner, M., Lappan, U., Stamm, M., Gerasimov, K.L., Beryozkina, T., Bakulev, V., et al. (2016). High conductivity in molecularly p-doped Diketopyrrolopyrrole-based polymer: the impact of a high dopant strength and good structural order. Adv. Mater. *28*, 6003–6010. https://doi.org/10.1002/adma.201506295.

28. Worfolk, B.J., Andrews, S.C., Park, S., Reinspach, J., Liu, N., Toney, M.F., Mannsfeld, S.C.B., and Bao, Z. (2015). Ultrahigh electrical conductivity in solution-sheared polymeric transparent films. Proc. Natl. Acad. Sci. USA. *112*, 14138–14143. https://doi.org/10.1073/pnas.1509958112.

29. El-Naggar, M.Y., Wanger, G., Leung, K.M., Yuzvinsky, T.D., Southam, G., Yang, J., Lau, W.M., Nealson, K.H., and Gorby, Y.A. (2010). Electrical transport along bacterial nanowires from Shewanella oneidensis MR-1. Proc. Natl. Acad. Sci. USA. *107*, 18127–18131. https://doi.org/10.1073/pnas.1004880107.

30. Rowe, A.R., Rajeev, P., Jain, A., Pirbadian, S., Okamoto, A., Gralnick, J.A., El-Naggar, M.Y., and Nealson, K.H. (2018). Tracking electron uptake from a cathode into shewanella cells: implications for energy acquisition from solid-substrate electron Donors. mBio 9, e02203–e02217. https://doi.org/10.1128/mBio.02203-17.

31. Sun, N., Youle, R.J., and Finkel, T. (2016). The mitochondrial basis of aging. Mol. Cell *61*, 654–666. https://doi.org/10.1016/j.molcel.2016.01.028.

32. Lehninger, A.L., Nelson, D.L., and Cox, M.M. (2004). Principles of Biochemistry (W. H. Freeman).

33. Yoshioka-Nishimura, M. (2016). Close relationships between the PSII repair cycle and thylakoid membrane Dynamics. Plant Cell Physiol. *57*, 1115–1122. https://doi.org/10.1093/pcp/pcw050.

34. Petrova, E.V., Korotkova, E.I., Kratochvil, B., Voronova, O.A., Dorozhko, E.V., and Bulycheva, E.V. (2014). Investigation of coenzyme Q10 by voltammetry. Procedia Chem. *10*, 173–178. https://doi.org/10.1016/j.proche.2014.10.030.

STAR★METHODS

KEY RESOURCES TABLE

REAGENT or RESOURCE	SOURCE	IDENTIFIER
Chemicals, peptides, and recombinant proteins		
PBS buffer, tablets	VWR Chemicals	97062-732
NaCl	VWR Chemicals	BDH9286
KCl	VWR Chemicals	BDH9258
2,3-dimethoxy-5-methyl-6-(farnesylfarnesyl)-1,4-benzo Quinone	Avanti Lipids	900150O-5 mg
Decamethyltetraconta-2,6,10,14,18,22,26,30,34,38-decaenyl]-5,6-dimethoxy-3-methylcyclohexa-2,5-diene-1,4-dione	Avanti Lipids	Currently not available
1,2-Distearoyl-sn-glycero-3-phosphoethanolamine	Avanti Lipids	850715P
1′,3′-bis[1,2-dioleoyl-sn-glycero-3-phospho] glycerol (sodium salt) (18:1, cardiolipin)	Avanti Lipids	710335P
Chloroform	VWR Chemicals	MK443210
Ethanol	VWR Chemicals	20821.321P

RESOURCE AVAILABILITY

Lead contact

Further information and requests for resources and reagents should be directed to and will be fulfilled by the Lead Contact, Dr Jakob Andersson (jakob.andersson@ait.ac.at).

Materials availability

This study did not generate any new unique materials.

Data and code availability

Data availability: all data will be made available via the data repository repositum.tuwien.ac.at upon reasonable request.

Code availability: this paper does not report original code.

Any additional information required to reanalyze the data reported in this paper is available from the lead contact upon request.

METHOD DETAILS

Key resources

Only commercially available resources were used for this study, available as detailed in the key resources table. Phosphate buffered saline (PBS) and other inorganic salts were obtained at p.A. quality (VWR). The lipids used were 2,3-dimethoxy-5-methyl-6-(farnesylfarnesyl)-1,4-benzo quinone (Q6, neat oil, extracted from *Saccharomyces cerevisiae*), purchased from Avanti Lipids (via Merck), Decamethyltetraconta-2,6,10,14,18,22,26,30,34,38-decaenyl]-5,6-dimethoxy3-methylcyclohexa-2,5-diene-1,4-dione (Q10), purchased from Avanti Lipids (via Merck), 1,2-Distearoyl-sn-glycero-3lipid mass concentrations of 0.1 mg/ml for Q6 and 0.25 mg/ml for DSPE. In addition Ethanol$\leq \geq \geq$99.9% pure from VWR and$\geq$ phosphoethanolamine (DSPE) as well as 1′,3′-bis[1,2-dioleoyl-sn-glycero-3-phospho] glycerol (sodium salt) (18:1, cardiolipin) were purchased from Avanti Polar Lipids. The lipids were dissolved in pure chloroform from Carl Roth (assay: 99.9%), with.

Milli-Q water (Milli-pore, TOC value 2 ppb, resistivity 18 MΩ) were used throughout for making solutions and for cleaning equipment. The defined volumes of lipid containing solutions of Q6 and DSPE, respectively, were dropped onto the water surface of an LBT (R & K, Potsdam, Germany) successively.

Langmuir - Blodgett transfer

The LB trough was filled with freshly prepared MilliQ-grade water (resistivity >18 MΩ· cm, total organic carbon 4 ppb). Lipids (or lipid mixtures) were dissolved in chloroform at 10 mg/mL and added dropwise to the LB trough. Droplets were release immediately above the water surface to avoid lipids "sinking" below the surface. Lipids were continuously added until a slight increase in pressure was observed, indicating that the surface was completely covered in lipid in the gas phase.

The lipid containing air/water interface was equilibrated for 10 minutes, and afterwards the lipid mixtures were compressed to 20 mN/m. Respective pressure/area characteristics are shown in Figure S1. At the set pressure of 20 mN/m the lipid bilayer was deposited by moving a chip out and into the sub-phase of the LBT at a speed of 22 $\mu m/s$. After bilayer formation the samples were never allowed to dry out or dewet. Therefore an 8 mm o-ring was glued around the electrodes prior to membrane deposition. MilliQ-grade water was used for making electrolyte solutions. PBS at pH 7 and 10 mM NaCl adjusted to pH 7 were used. For a schematic of the LB-film transfer method, see Figure S1.

Chip production

Oxidized silicon wafers (100 nm oxide) were cleaned for 1h in concentrated acidic piranha (1:3 30% hydrogen peroxide/98% sulphuric acid), rinsed thoroughly with MilliQ-grade water followed by ethanol. A 5 nm of Ti adhesion layer was added via sputter coating, and 50 nm of gold was deposited by evaporation under constant rotation. Sputtering and evaporation were done in the same custom-built setup such that the Ti adhesion layer was not exposed to air before gold deposition. Sputtering and evaporation took place at a pressure of of $2 \cdot 10^{-6}$mbar.

Electrode shapes were defined by masking the chips using a custom-built evaporation mask. The designed mask generates two gold electrodes that are separated by a 30 μm gap, which was measured by SEM, over roughly 0.5 mm distance. The area of the working-and counter electrode under the droplet is roughly 0.5 mm^2. Using Langmuir-Blodgett trough (LBT) deposition a membrane can be grafted on this chip, so that an *in-plane* resistance can be measured. An o-ring prevents drying out of the membrane and stabilize the droplet. The diameter of the o-ring is selected such that the area of the electrode remains small, but large enough that wetting effects (contact angle formation) should not impact the deposition of the membrane during transfer across the air/water interface in the LBT. The corresponding transfer ratio is between 0.9 - 1.

Electrochemistry

All electrochemical experiments were done using either a Pt-wire or Ag-AgCl-electrode as reference electrodes with a PalmSense or a Biologic potentiostatic. Data is referenced to the Ag|AgCl potential. All electrodes were rinsed thoroughly with ethanol followed by MilliQ-grade water prior to use. The distance between working electrode (or source and drain electrodes) was kept as constant as possible around 0.5 cm. All experiments were done in 1X PBS at pH 7.4.

A redox potential of +650 mV is established between the working (WE) and reference (RE) electrode, while the counter electrode (CE 1) can supply in plane membrane current. The current is measured laterally across Q-containing membranes as shown in the schematic, which effectively enables an in-plane current between the WE and CE 1. CE 1 supplies the current consumed by the WE in a potentiostatic setup. At the same time a pH gradient is established due to simultaneous proton hoping. Control experiments include insulating membranes without Q-lipids, blank chips as well as measurements with the redox active membranes using an alternative counter electrode (CE 2, platinum). CE 2 cannot establish trans membrane current flow as it inserts into the electrolyte without direct membrane contact. To avoid drying out of the membrane, buffer solution was replenished during the experiment as needed.

We also tested the redox behaviour of dissolved Q-lipid (saturated solution) and compared it to literature (Figure S10). We observed an oxidation peak occurring around 0.3–0.4 V, which is in agreement with previous reports of Q-lipid redox behaviour,[34] and as expected for quinone oxidation in general. As observed in literature, reduction occurred at −0.5V indicative of significant over potentials for the reduction.[16,17,34] This may be due to complex micelle formations in solution, and is not of interest for this work, where 2D in-plane characteristics are compared.

In-plane conductivity of lipid monolayer at the air-water interface of a Langmuir-Blodgett-Trough

Measurements were conducted by dipping two platinum plates into the Langmuir Blodgett trough in deoxygenated MilliQ-grade water (18.2 MΩ) was used. These experiments were carried out with a deoxygenated MilliQ-grade water sub phase (obtained immediately prior to the experiment) instead of an electrolyte, as the high electrolyte conductivity would obscure the in-plane currents in the nA-range. Electrodes were inserted into the trough prior to the addition of any lipid mixtures to ensure contact was made at the air-water interface.

Atomic force microscopy

AFM topography experiments were performed using an environmental Cypher (Asylum Research) and triangular high-frequency cantilevers that are driven by photo thermal excitation. Using a custom-made cell, providing a well for holding liquid, lipid bilayers were deposited and never allowed to dry out or dewet prior to measurements. The well was made by stamping a UV glue well with an o-ring onto muscovite mica sheet where the previously mentioned electrodes were deposited.

QUANTIFICATION AND STATISTICAL ANALYSIS

Errors of the parameters fitted to the electrochemical impedance data are the values produced by the fitting program ZView4 which indicate the range of values that could be used for each element without decreasing the quality of the fit (based on least squares analysis).